RSC Advances

PAPER

View Article Online
View Journal | View Issue

Cite this: *RSC Adv.*, 2020, **10**, 38281

A naphthalimide-based turn-on fluorescence probe for peroxynitrite detection and imaging in living cells†

Xiling Liu,[b] Fangyuan Gu,[c] Xinyi Zhou,[b] Wei Zhou,*[a] Shuping Zhang,[b] Lei Cui[c] and Ting Guo *[a]

Received 29th July 2020
Accepted 11th October 2020

DOI: 10.1039/d0ra06564a

rsc.li/rsc-advances

Peroxynitrite ($ONOO^-$) is a potent biological oxidant that plays a significant role in diverse physiological and pathological processes. A novel fluorescent probe **HCA-OH** was developed for specific and sensitive detection of peroxynitrite, and displayed a significant fluorescence turn-on signal. With low cytotoxicity and good photostability, the probe **HCA-OH** could be applied in imaging $ONOO^-$ distribution in HepG2 cells and live *C. elegans* in real time. Therefore, the probe can be a promising tool for imaging *in vivo*.

Introduction

Peroxynitrite ($ONOO^-$) is one of the most powerful oxidants among reactive nitrogen species (RNS), which is formed from the reaction between nitric oxide (NO) and superoxide radical anion ($O_2^{\bullet -}$) under physiological conditions.[1–4] The highly reactive peroxynitrite can oxidize or nitrate amino acid residues of proteins, such as tyrosine, cysteine, methionine and tryptophan. Modifications of these amino acids potentially alter the protein's function, inducing various diseases.[5,6] Peroxynitrite can also oxidize sugars and damage DNA.[7] The production and scavenging of peroxynitrite are correlated with the energy metabolism in tumor cells.[8] Therefore, robust detection of peroxynitrite in living organisms is useful for understanding its roles in disease pathophysiology.

Fluorescent technique is indispensable in biological imaging.[9–16] Because of high selectivity, rapid response and low toxicity, fluorescent probes have been developed for a wide range of substrates, including $ONOO^-$.[17–23] Qian's group developed a near-infrared fluorescent probe ONP to track endogenous $ONOO^-$ in brains of kainate-induced epileptic seizures.[24] Zhang *et al.* proposed a novel approach for developing stable NIR fluorochromic platform, which was applied in design of NIR fluorescent probes for monitoring $ONOO^-$ and evaluating hepatotoxicity.[25] Xie and co-workers developed a formamide group as the special trigger for peroxynitrite.[26] However, fluorescent probe for $ONOO^-$ imaging are typically restricted for cell based imaging studies. It would be a significant step forward to further develop probes for whole organism, for which *C. elegans* was an excellent and wide-accessible model.[27–29]

In this paper, a novel fluorescent probe **HCA-OH** is designed by tethering *p*-aminophenol to 1,8-naphthalimide directly (Scheme 1). The *p*-aminophenol moiety has been proved to be an oxidant-sensitive moiety *via* *N*-/*O*-dearylation.[30–33] 1,8-naphthalimide fluorophore was used due to its good photostability and high fluorescence quantum yield.[34] Upon oxidation of $ONOO^-$, the probe **HCA-OH** could release the fluorophore **HCA-NH$_2$** and the fluorescence was restored. The probe **HCA-OH** was readily synthesized through in two steps (Scheme 2). Its structure was confirmed by ^{1}H- and ^{13}C-NMR and HRMS. We also obtained the single crystal structure of the probe **HCA-OH** (Table S1†).

Experimental section

General procedure

Chemical reagents and solvents applied in this work were purchased from commercial suppliers and directly used

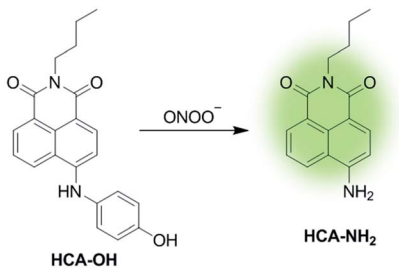

Scheme 1 Structure and mechanism of **HCA-OH** for $ONOO^-$.

[a]College of Pharmaceutical Sciences, Southwest University, Chongqing 400715, China. E-mail: guoting15@swu.edu.cn

[b]College of Science, University of Shanghai for Science and Technology, Shanghai 200093, China

[c]College of Science, Shanghai University, Shanghai 200444, China

† Electronic supplementary information (ESI) available. CCDC 1974831. For ESI and crystallographic data in CIF or other electronic format see DOI: 10.1039/d0ra06564a

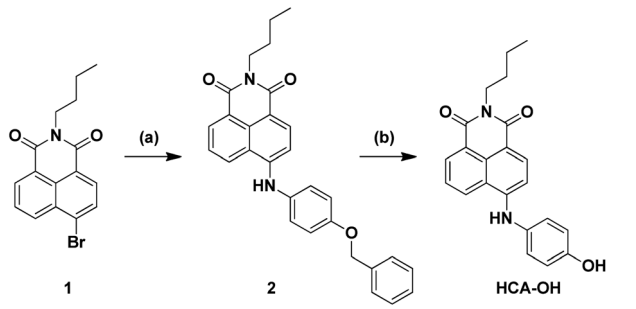

Scheme 2 Synthetic route of probe **HCA-OH**. Reagents and conditions: (a) 4-benzyloxy aniline, BINAP, Pd $(dba)_3$, *t*-BuONa, toluene, 90 °C, 12 h. (b) BBr_3, CH_2Cl_2, 6 h.

without further purification. High resolution mass spectra (HRMS) were recorded using a LC-MS 2010A (Shimadzu) instrument. ^{1}H NMR and ^{13}C NMR spectra were measured on a Bruker AV-500 NMR spectrometer. Absorption spectra were operated on a UV-2501PC spectrophotometer. Fluorescence emission spectra were measured on a RF-5301PC spectrophotometer. The fluorescence images of cells and *C. elegans* were obtained using ZOE™ Fluorescent Cell Imager (1450031EDU) by Bio-Rad.

Synthesis of compound 2

A mixture of compound **1** (700.0 mg, 2.11 mmol), 4-benzyloxy aniline (400.0 mg, 2.0 mmol), BINAP (65.0 mg, 0.11 mmol), $Pd(dba)_3$ (18.0 mg, 0.02 mmol) and sodium tertiary butoxide (960.0 mg, 9.99 mmol) were dissolved in 20 mL toluene in a single necked flask. The reaction mixture was heated to 90 °C and stirred for 12 h. After cooling to room temperature, the solution was removed under reduced pressure. The residue was dissolved in ethyl acetate and washed with brine tree times, then dried over Na_2SO_4. After filtered and concentrated, the crude product was purified by flash silica gel chromatography (ethyl acetate/petroleum ether = 1/6) to obtain compound **2** (710 mg, 75%). ^{1}H NMR (500 MHz, $CDCl_3$) δ 8.60 (dd, J = 8.6, 1.0 Hz, 1H), 8.37 (d, J = 8.4 Hz, 1H), 8.26 (dd, J = 8.4, 1.0 Hz, 1H), 7.68 (dd, J = 7.78, 4.16 Hz, 1H), 7.47 (d, J = 7.0 Hz, 2H), 7.43–7.40 (m, 2H), 7.37–7.34 (m, 1H), 7.25 (d, J = 2.0 Hz, 1H), 7.24 (d, J = 2.0 Hz, 1H), 7.06 (d, J = 2.0 Hz, 1H), 7.05 (d, J = 2.2 Hz, 1H), 7.02 (d, J = 8.42 Hz, 1H), 6.78 (s, 1H), 5.11 (s, 2H), 4.17–4.14 (m, 2H), 1.74–1.67 (m, 2H), 1.46 (dd, J = 15.2, 7.5 Hz, 2H), 0.99 (t, J = 7.4 Hz, 3H). ^{13}C NMR (125 MHz, $CDCl_3$) δ 164.60, 164.07, 154.61, 153.09, 144.86, 137.05, 132.68, 131.54, 131.07, 130.29, 128.71, 128.14, 127.62, 126.68, 125.63, 123.29, 122.31, 118.77, 117.20, 116.03, 70.54, 43.30, 40.22, 30.41, 20.55, 14.00.

Synthesis of probe HCA-OH

Compound **2** (30.0 mg, 0.067 mmol) was dissolved in 3 mL of CH_2Cl_2, then BBr_3 (50.0 mg, 0.2 mmol) was slowly added to the mixture. The reaction was stirred in an ice-water bath for 6 h and monitored by TLC analysis. After all starting material got consumed, water was added to quench the reaction, and filtered. Compound **HCA-OH** was obtained as a red solid (20.0 mg, 83%).

^{1}H NMR (500 MHz, DMSO-d_6) δ 9.54 (s, 1H), 9.20 (s, 1H), 8.76 (d, J = 8.0 Hz, 1H), 8.40 (d, J = 7.0 Hz, 1H), 8.14 (d, J = 8.5 Hz, 1H), 7.68 (t, J = 8.0 Hz, 1H), 7.18 (d, J = 8.5 Hz, 2H), 6.87 (d, J = 8.5 Hz, 2H), 6.82 (d, J = 8.5 Hz, 1H), 3.96–3.95 (m, 2H), 1.58–1.52 (m, 2H), 1.34–1.27 (m, 2H), 0.89 (t, J = 7.5 Hz, 3H). ^{13}C NMR (125 MHz, DMSO-d_6) δ 163.65, 162.77, 155.21, 149.69, 133.65, 130.77, 129.48, 128.67, 126.39, 124.61, 121.87, 120.56, 116.15, 109.32, 105.99, 39.02, 29.79, 19.84, 13.74 HRMS (ESI) (m/z): $[M + H]^+$ calcd for $C_{22}H_{21}N_2O_3$ 361.1547; found, 361.1543.

General procedure for $ONOO^-$ detection

All fluorescence measurements were performed in 10 mM PBS buffer (pH 7.4, containing 1% DMSO). Fluorescence titration studies were performed by addition of an aliquot stock solution of various interfering species into **HCA-OH** solution. The mixture solution was incubated at 37 °C for 20 min before tested. Samples for absorption and fluorescence measurements were contained in 1 cm × 1 cm quartz cuvettes (3.5 mL volume). Excitation wavelength was 460 nm. The excitation and emission slits were 5 nm.

Culture of cell and *C. elegans*

HepG2 cells were cultured in Dulbecco's modified Eagle's medium (DMEM) supplemented with 10% fetal bovine serum (FBS) at 37 °C in a humidified atmosphere of 95% air (20% O_2) and 5% CO_2. For probe loading, the cells were washed with D-Hanks and then incubated with 3 μM **HCA-OH** (containing 1% DMSO in serum-free DMEM) for 45 min at 37 °C. For imaging the exogenous $ONOO^-$, the cells were pre-treat with $ONOO^-$ solutions (15 and 30 μM, respectively) for 1 h in DMEM medium at 37 °C and washed three times with pre-warmed PBS buffer, then incubated with probe **HCA-OH** (3 μM) 1 h at 37 °C. Last, cells were washed with pre-warmed PBS buffer three times for cell imaging.

The larval stage 4 (L4) *C. elegans* was first washed with M9 three times by centrifugation at 3200 rpm for 3 min. Then the *C. elegans* was divided into three groups, every group was incubated with 1000 μL M9 and **HCA-OH** (final concentration 3 μM) at 20 °C for 2 h. To expose the *C. elegans* to $ONOO^-$, different amounts of $ONOO^-$ were added to each group and the groups incubated for another 2 h. Before imaging, the *C. elegans* were washed three times with M9, then centrifuged at 3200 rpm for 3 min.

Cytotoxicity assay of probe

HepG2 cells (5×10^4 cells per mL) were planted in 96-well plates in DMEM with 10% FBS for 24 h (5% CO_2/95% air, 37 °C). Next, plates were incubated in different concentrations of the probe from 0 μM to 320 μM (containing 1% DMSO in 100 μL DMEM). Subsequently, MTT solution (5.0 mg mL^{-1}, PBS) was added to each well and diluted 10 times before added. Then cells were incubated for 4 h under the same conditions and 150 μL DMSO was added in each well. After 10 min of shaking, the absorbance was measured at 490 nm using a microplate reader.

Results and discussion

Fluorescence detection of $ONOO^-$

The reactivity of **HCA-OH** toward $ONOO^-$ were carried out in PBS (10 mM, pH 7.4, 1% DMSO). Without $ONOO^-$, the free probe **HCA-OH** was almost non-fluorescent. Upon addition of $ONOO^-$, the probe **HCA-OH** showed a dramatic fluorescent enhancement at 548 nm, and the absorption maxima blue-shifted from 460 nm to 431 nm (Fig. 1a and S2†). This suggested that the *p*-aminophenol moiety of the probe was oxidized and N-dearylated and the fluorophore **HCA-NH$_2$** was generated.

The dose-dependent spectral response between the concentration of $ONOO^-$ and fluorescence intensity at 548 nm was also studied (Fig. 1b). Fluorescence response of **HCA-OH** to $ONOO^-$ displayed a linear relationship ($R^2 = 0.991$) in the range of 10 to 80 μM. And the limit of detection (LOD), calculated according to the $3\sigma/K$, where K is the slope of the calibration curve and σ is the standard deviation ($n = 11$), is estimated to be 49.7 nM. The probe also showed a time dependent fluorescent enhancement. Fluorescence intensity increased immediately after the addition of $ONOO^-$ and reached the plateau within 12 min (Fig. 2), which remained stable in further 170 nm (Fig. S3†). These results indicated that the probe **HCA-OH** could sensitively detect $ONOO^-$ under physiological conditions.

Mechanism study

LC-MS was used to explore the mechanism of **HCA-OH** oxidation (Fig. S4†). The pure probe **HCA-OH** and fluorophore **HCA-NH$_2$** were tested as control, which showed peaks with retention time at 1.63 min and 3.87 min, respectively. The reaction solutions of the probe **HCA-OH** and $ONOO^-$ were mixed and incubated for 10 min and 20 min respectively, before injection for analysis. With the extension of reaction time, the peak of **HCA-OH** in 1.63 min decreased and the peak of **HCA-NH$_2$** in 3.87 min increased gradually. The MS spectroscopy showed appearance of a new peak of at m/z 269.2, which was consistent with the $[\textbf{HCA-NH}_2 + H]^+$. These results confirmed that the fluorophore **HCA-NH$_2$** was released from the probe by the oxidation of $ONOO^-$.

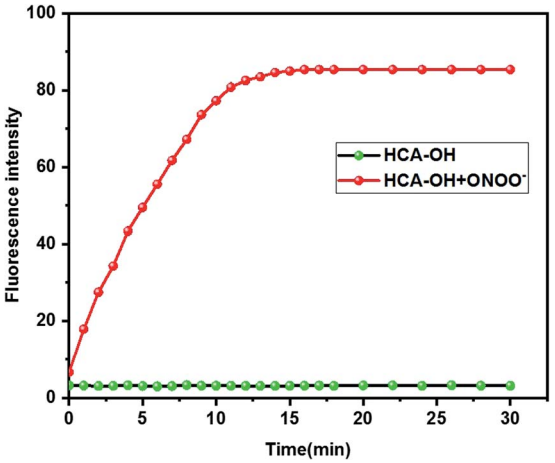

Fig. 2 Time-dependent changes in the fluorescence intensity of HCA-OH (black line: 0 μM $ONOO^-$, red line: 30 μM $ONOO^-$). The excitation and emission wavelength were 460 nm and 548 nm, respectively.

To further study the nature of the electronic transitions and electronic structures of **HCA-OH**, time-dependent density functional theory (TD-DFT) calculations on molecular orbital distribution of optimized structures of **HCA-OH** were carried out at B3LYP/6–311++g(d.p) (Fig. 3 and Table S2†). The calculation results of the S_0 states indicated that the major low-energy absorptions were predominantly involved in the electronic transitions from the HOMO to LUMO. The HOMO for the calculated compound were mainly localized on the naphthalimide nucleus and phenol, and the LUMO were populated on the naphthalimide moiety. The proportion of the S_0 state's phenol moiety in the LUMO increased up to 70% compared to that in the HOMO, indicating that the low-energy electronic transitions for the **HCA-OH** originated from π–π* electronic transitions. Furthermore, the theoretical results for the S_1 optimized structures of this compound showed that the major contribution to the low-energy emission was associated with a HOMO → LUMO transition. These results also revealed the π–π* transitions to exhibit considerable ICT character, which

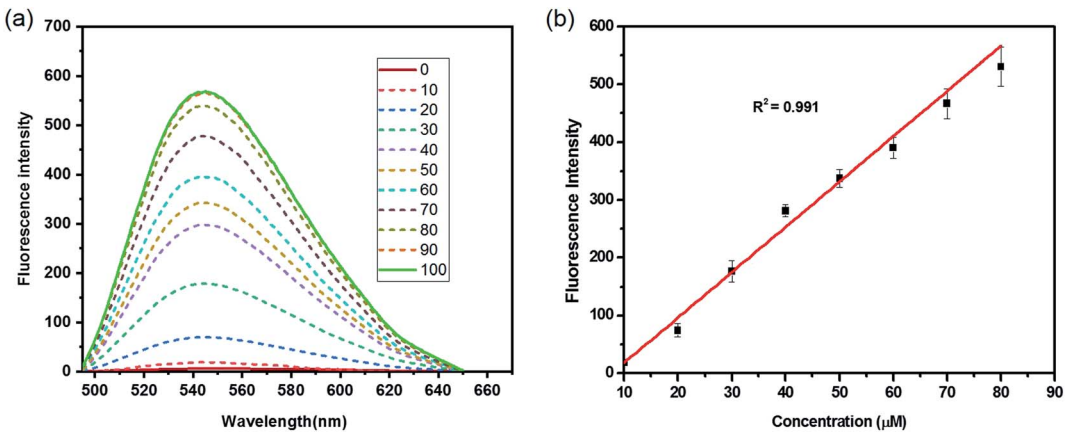

Fig. 1 (a) Fluorescence spectra of HCA-OH (10 μM) with $ONOO^-$ titration (0–100 μM). (b) Linear–correlation between fluorescence intensity of HCA-OH at 548 nm and concentrations of $ONOO^-$ (0–80 μM). The excitation wavelength was 460 nm.

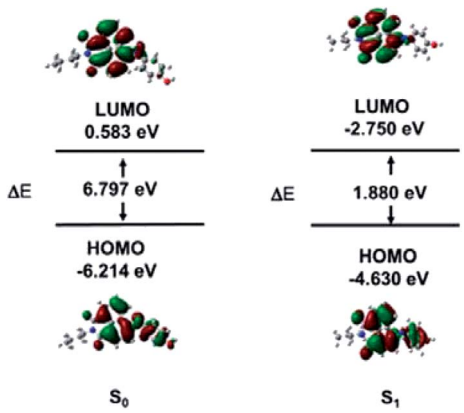

Fig. 3 HOMO and LUMO of **HCA-OH** obtained by DFT method.

were identical to the phenomena observed for the S_0 optimized structures of this compound. The difference in the HOMO energies between S_0 state and S_1 state is 1.584 eV, whereas the difference in the LUMO energies are 3.333 eV. The energy gap in S_0 state is 6.797 eV, whereas it is only 1.880 eV in S_1 state.

In addition, the theoretical calculation results exhibited that the contributions of the –NH– to HOMO levels as well as the electronic effects of phenol to LUMO levels distinctly demonstrate that fluorescence color of compound can be systematically tuned.

Selectivity of probe HCA-OH and the effect of pH

The selectivity of probe **HCA-OH** was investigated. The probe **HCA-OH** was treated with various potentially interfering species in PBS buffer (10 mM, pH 7.4, 1% DMSO) at 37 °C. As shown in Fig. 4, $ONOO^-$ induced a significant fluorescence enhancement at 548 nm. In contrast, other species, including Na^+, K^+, Mg^{2+}, Cu^{2+}, Fe^{2+}, Fe^{3+}, Ca^{2+}, Cl^-, $S_2O_3^{2-}$, SO_4^{2-}, HSO_3^-, NO_3^-, Cys, HCy, GSH, $^{\bullet}OH$, *t*-BuOOH, $^1O_2$, NO, NO_2^-, H_2O_2, $O_2^{\bullet-}$, ClO^-, induced nearly no fluorescence changes even after 20 min at 37 °C.

These results showed that the probe could be used to specially detect $ONOO^-$ in presence of other biological species. The effect of pH on the response of the probe to $ONOO^-$ was also investigated (Fig. S5†). The fluorescence intensity of the probe **HCA-OH** at 548 nm remained weak from the pH range of 2.0 to 11.0. And a bright fluorescence of the reaction product between the probe and $ONOO^-$ was also insensitive to pH in the range of 2 to 11.0, indicating that the detection of $ONOO^-$ by the probe could not be effected by the pH value. The excellent selectivity and pH-insensitivity verified that the probe **HCA-OH** has great potential in living imaging.

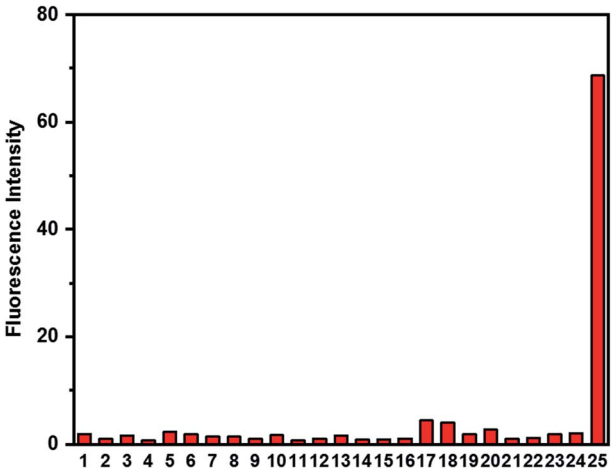

Fig. 4 Fluorescence responses of **HCA-OH** toward 100 μM analytes unless otherwise noted: (1) blank, (2) Na^+, (3) K^+, (4) Mg^{2+}, (5) Cu^{2+}, (6) Fe^{2+}, (7) Fe^{3+}, (8) Ca^{2+}, (9) Cl^-, (10) $S_2O_3^{2-}$, (11) SO_4^{2-}, (12) HSO_3^-, (13) NO_3^-, (14) Cys (5 mM), (15) HCy (5 mM), (16) GSH (5 mM), (17) $^{\bullet}OH$, (18) *t*-BuOOH, (19) $^1O_2$, (20) NO, (21) NO_2^-, (22) H_2O_2, (23) $O_2^{\bullet-}$, (24) ClO^-, (25) $ONOO^-$ (30 μM). The final concentration of **HCA-OH** was 10 μM. All experiments data were collected in PBS buffer (10 mM, pH 7.4) with 1% DMSO at 37 °C. The excitation and emission wavelength were 460 nm and 548 nm, respectively.

Fluorescence imaging of exogenous $ONOO^-$ in HepG2

We evaluated the cytotoxicity of the probe **HCA-OH** (0–320 μM) in HepG2 cells. The MTT assay showed that the probe **HCA-OH** displayed low cytotoxicity (Fig. S6†). Then, the probe **HCA-OH** was applied to detect intracellular $ONOO^-$ in HepG2 cells. As showed in Fig. 5d, HepG2 cells incubated only with the probe **HCA-OH** (3 μM) displayed ignorable fluorescence. In contrast, HepG2 cells pretreated with $ONOO^-$ (15 μM and 30 μM, respectively) showed a remarkable fluorescence enhancement (Fig. 5e and f). An average emission value of fluorescent photos at different concentrations of $ONOO^-$ were obtained. The emission intensity of cells was promoted by 30 μM $ONOO^-$ than

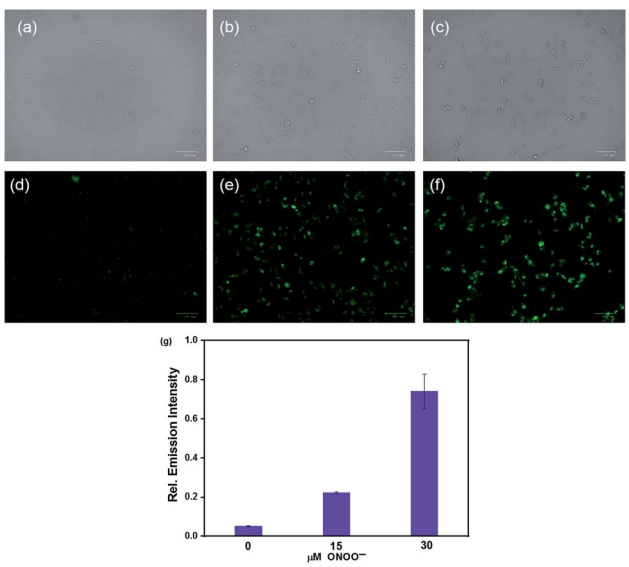

Fig. 5 Fluorescent imaging of exogenous $ONOO^-$ in HepG2 cells. Top: bright field images. Bottom: fluorescent images. (a and d) Cells were incubated with probe **HCA-OH** (3 μM) as control (b and e) Cells were incubated with the probe **HCA-OH** (3 μM) and $ONOO^-$ (15 μM). (c and f) Cells were incubated with the probe **HCA-OH** (3 μM) and $ONOO^-$ (30 μM). (g) Mean fluorescence intensity of images. The excitation wavelength was 463–497 nm, and the fluorescent emissions were collected from 430 to 495 nm window.

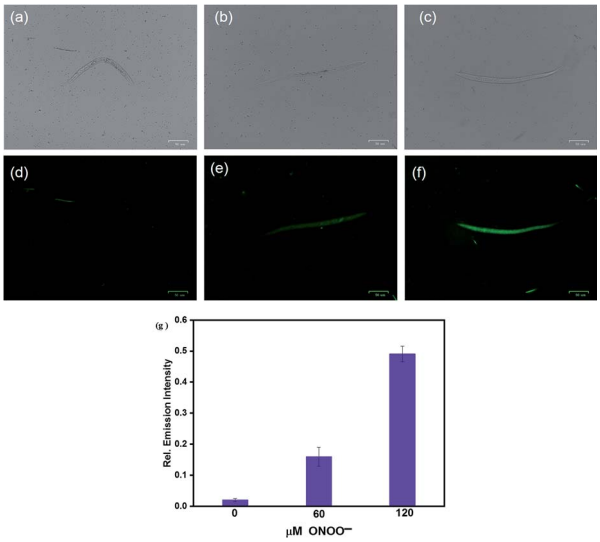

Fig. 6 Fluorescent imaging of $ONOO^-$ in *C. elegans*. Top: bright field images. Bottom: fluorescent images. (a and d) *C. elegans* were incubated with probe **HCA-OH** (3 μM). (b and e) *C. elegans* were incubated with probe **HCA-OH** (3 μM) and $ONOO^-$ (60 μM). (c and f) *C. elegans* were incubated with probe **HCA-OH** (3 μM) and $ONOO^-$ (120 μM). (g) Mean fluorescence intensity of images. The excitation wavelength was 463–497 nm, and the fluorescent emissions were collected from 430 to 495 nm window.

15 μM $ONOO^-$ (Fig. 4g). These results demonstrated that **HCA-OH** could be used for detection of $ONOO^-$ in living cells.

Imaging of $ONOO^-$ in *C. elegans*

The excellent fluorescence properties of **HCA-OH** prompted us to test its potential application for imaging $ONOO^-$ in living *C. elegans*. *C. elegans* were incubated with **HCA-OH** (3 μM) for 2 h, a weak fluorescence was observed in the green channel (Fig. 6d). Whereas, addition of $ONOO^-$ leaded the appearance of fluorescence signals. With the increase of $ONOO^-$ concentration, the fluorescence became much brighter (Fig. 6e and f), indicating that **HCA-OH** could be absorbed by the *C. elegans* and distributed throughout the whole organism. We quantified the relative fluorescence intensity of images at different $ONOO^-$ concentration. A dose-dependent fluorescence intensity enhancement was clearly exhibited (Fig. 6g). These results revealed that **HCA-OH** could be a suitable probe to monitor $ONOO^-$ in *C. elegans*.

Conclusions

In summary, we have developed a novel naphthallimide-based fluorescent probe **HCA-OH** for $ONOO^-$. The good stability of its fluorescence towards the pH from 2.0 to 11.0 made the probe can be used in physiological condition. With a dramatic fluorescent turn-on signal, the fluorescent probe could sensitively detect $ONOO^-$ over other ROS/RNS. In addition, the probe **HCA-OH**, possessing good cell permeability and low cytotoxicity, was suitable for monitor $ONOO^-$ in *C. elegans* and HepG2 cells. Therefore, the probe **HCA-OH** has potential application for imaging in living organisms.

Conflicts of interest

There are no conflicts to declare.

Acknowledgements

The work was supported by the National Natural Science Foundation of China (grant number 21602181, 21702171) and China Postdoctoral Science Foundation (grant number 2016M602628).

Notes and references

1 C. Szabo, H. Ischiropoulos and R. Radi, *Nat. Rev. Drug Discovery*, 2007, **6**, 662–680.
2 A. Kamm, P. Przychodzen, A. Kuban-Jankowska, D. Jacewicz, A. M. Dabrowska, S. Nussberger, M. Wozniak and M. Gorska-Ponikowska, *Nitric Oxide*, 2019, **93**, 102–114.
3 R. Radi, *Proc. Natl. Acad. Sci. U. S. A.*, 2018, **115**, 5839–5848.
4 P. Pacher, J. S. Beckman and L. Liaudet, *Physiol. Rev.*, 2007, **87**, 315–424.
5 J. S. Beckman and W. H. Koppenol, *Am. J. Physiol.*, 1996, **271**, C1424–C1437.
6 R. Radi, *J. Biol. Chem.*, 2013, **288**, 26464–26472.
7 L. J. Ignarro and B. A. Freeman, *Nitric Oxide: Biology and Pathobiology*, Academic Press Ltd-Elsevier Science Ltd, London, 3th edn, 2017.
8 J. C. Pestoni, S. Klingeman Plati, O. D. Valdivia Camacho, M. A. Fuse, M. Onatunde, N. A. Sparrow, M. A. Karajannis, C. Fernandez-Valle and M. C. Franco, *J. Biol. Chem.*, 2019, **294**, 11354–11368.
9 Q. Gong, W. Shi, L. Li and H. Ma, *Chem. Sci.*, 2016, **7**, 788–792.
10 C. Y. Wang, S. P. Zhang, J. H. Huang, L. Cui, J. Hu and S. Y. Tan, *RSC Adv.*, 2019, **9**, 21572–21577.
11 J. Lv, F. Wang, J. Qiang, X. Ren, Y. Chen, Z. Zhang, Y. Wang, W. Zhang and X. Chen, *Biosens. Bioelectron.*, 2017, **87**, 96–100.
12 L. Wu, A. C. Sedgwick, X. Sun, S. D. Bull, X.-P. He and T. D. James, *Acc. Chem. Res.*, 2019, **52**, 2582–2597.
13 T. C. Pham, Y. K. Kim, J. B. Park, S. Jeon, J. Ahn, Y. Yim, J. Yoon and S. Lee, *ChemPhotoChem*, 2019, **3**, 1133–1137.
14 Y. Chen, T. Wei, Z. Zhang, W. Zhang, J. Lv, T. Chen, B. Chi, F. Wang and X. Chen, *Chin. Chem. Lett.*, 2017, **28**, 1957–1960.
15 C. Chang, F. Wang, J. Qiang, Z. Zhang, Y. Chen, W. Zhang, Y. Wang and X. Chen, *Sens. Actuators, B*, 2017, **243**, 22–28.
16 J. Lv, Y. Chen, F. Wang, T. Wei, Z. Zhang, J. Qiang and X. Chen, *Dyes Pigm.*, 2018, **148**, 353–358.
17 X. Chen, X. Tian, I. Shin and J. Yoon, *Chem. Soc. Rev.*, 2011, **40**, 4783–4804.
18 X. Chen, F. Wang, J. Y. Hyun, T. Wei, J. Qiang, X. Ren, I. Shin and J. Yoon, *Chem. Soc. Rev.*, 2016, **45**, 2976–3016.
19 M. Zhu, H. Zhou, D. Ji, G. Li, F. Wang, D. Song, B. Deng, C. Li and R. Qiao, *Dyes Pigm.*, 2019, **168**, 77–83.

20 Z. Wang, L. Wu, Y. Wang, M. Zhang, Z. Zhao, C. Liu, Q. Duan, P. Jia and B. Zhu, *Anal. Chim. Acta*, 2019, **1049**, 219–225.
21 W. Shu, Y. Wu, T. Shen, J. Cui, H. Kang, J. Jing and X. Zhang, *Dyes Pigm.*, 2019, **170**, 107609.
22 Y. Shen, M. Li, M. Yang, Y. Zhang, H. Li and X. Zhang, *Spectrochim. Acta, Part A*, 2019, **222**, 117230.
23 Z. Li, C. Liu, C. Yu, Y. Chen, P. Jia, H. Zhu, X. Zhang, Y. Yu, B. Zhu and W. Sheng, *Analyst*, 2019, **144**, 3442–3449.
24 J. S. Hu, C. Shao, X. Wang, X. Di, X. Xue, Z. Su, J. Zhao, H. L. Zhu, H. K. Liu and Y. Qian, *Adv. Sci.*, 2019, **6**, 1900341.
25 D. Cheng, J. Peng, Y. Lv, D. Su, D. Liu, M. Chen, L. Yuan and X. Zhang, *J. Am. Chem. Soc.*, 2019, **141**, 6352–6361.
26 X. Xie, G. Liu, X. Su, Y. Li, Y. Liu, X. Jiao, X. Wang and B. Tang, *Anal. Chem.*, 2019, **91**, 6872–6879.
27 A. Miranda-Vizuete and E. A. Veal, *Redox Biol.*, 2017, **11**, 708–714.
28 C. F. Labuschagne and A. B. Brenkman, *Ageing Res. Rev.*, 2013, **12**, 918–930.
29 D. Shi, S. Chen, B. Dong, Y. Zhang, C. Sheng, T. D. James and Y. Guo, *Chem. Sci.*, 2019, **10**, 3715–3722.
30 R. K. Jackson, Y. Shi, X. Yao and S. C. Burdette, *Dalton Trans.*, 2010, **39**, 4155–4161.
31 T. Peng, N.-K. Wong, X. Chen, Y.-K. Chan, D. H.-H. Ho, Z. Sun, J. J. Hu, J. Shen, H. El-Nezami and D. Yang, *J. Am. Chem. Soc.*, 2014, **136**, 11728–11734.
32 X. Li, J. Hou, C. Peng, L. Chen, W. Liu and Y. Liu, *RSC Adv.*, 2017, **7**, 34287–34292.
33 X. Song, W. Hu, D. Wang, Z. Mao and Z. Liu, *Analyst*, 2019, **144**, 3546–3551.
34 R. M. Duke, E. B. Veale, F. M. Pfeffer, P. E. Kruger and T. Gunnlaugsson, *Chem. Soc. Rev.*, 2010, **39**, 3936–3953.